J Mater Sci (2011) 46:5621–5627
DOI 10.1007/s10853-011-5512-x

Piezoelectric BNT-$BT_{0.11}$ thin films processed by sol–gel technique

Marin Cernea · Aurelian Catalin Galca · Marius Cristian Cioangher · Cristina Dragoi · Gelu Ioncea

Received: 30 November 2010 / Accepted: 25 March 2011 / Published online: 5 April 2011

Abstract $0.89(Na_{0.5}Bi_{0.5})TiO_3$–$0.11BaTiO_3$, (BNT-$BT_{0.11}$) thin film was fabricated by sol–gel/spin coating process, on platinized silicon wafer. Perovskite structure with random orientation of crystallites has been obtained at 700 °C. Piezoelectric activity of BNT-$BT_{0.11}$ thin film was detected using piezoresponse force microscopy (PFM). Effective piezoelectric coefficient d_{33eff} of such film, recorded at 5 V applied dc voltage, was ~29 pm/V, which is similar to other BNT-BT_x thin films. The complex refractive index and dielectric function of BNT-$BT_{0.11}$ thin films were also investigated. The high leakage current density significantly influences the dielectric, ferroelectric, and piezoelectric properties of the BNT-$BT_{0.11}$ films.

Introduction

BNT-based ceramics are studied as lead-free piezoelectric materials to replace lead-containing piezoelectric ceramics [1, 2]. The addition of $BaTiO_3$ to $(Bi_{0.5}Na_{0.5})TiO_3$ improves the piezoelectric and sintering properties [3, 4]. Among these BNT-based solid solutions $(Na_{0.5}Bi_{0.5})TiO_3$–$BaTiO_3$ (BNT-BT) system is most attractive due to its excellent piezoelectric properties, which exists as morphotropic phase boundary (MPB) between the rhombohedral phase (BNT) and the tetragonal phase (BT) [4–8]. Many significant research results of BNT-BT system in MPB region were reported. Various compositional ranges of the MPB have been reported for $(1 - x)$BNT-(x)BT (BNT-BT_x) ceramics, such as $x = 0.06$–0.07 [5] and $0.04 < x < 0.06$ [6]. Chen et al. [7], report that it can be inferred that the MPB of NBT-(x)BT ceramics lies in the composition range of $0.06 \leq x \leq 0.10$ at room temperature and the tetragonal single phase exists at $x \geq 12$. Other references [4, 8], propose that the MPB lies at the composition of $x \sim 5.5$. The discrepancies observed in determining the exact MPB composition of the BNT-BT solid solution system between various results reported may be related to different preparation methods or processing parameters employed by different groups. Processing and properties of BNT-BT_x bulk ceramics have been extensively reported [5, 9–12]. However, few reports on BNT-BT_x thin films were published. These BNT-BT_x thin films have been prepared by: chemical solution deposition [11], solid-state reaction [13, 14], pulsed laser deposition [15–17], and metal–organic decomposition [18].

In this article, we report on the synthesis of BNT-$BT_{0.11}$ precursor sol and the crystallization of BNT-$BT_{0.08}$ thin films, deposited by spin-coating method on $Pt/TiO_2/SiO_2/Si$ substrates. The microstructures, optical, dielectric, and piezoelectric properties of the films are investigated.

Experimental procedure

Precursor sol of $0.89[(Bi_{0.5}Na_{0.5})TiO_3]$–$0.11[BaTiO_3]$ was prepared by an acetate-alkoxide sol–gel technique. Production of the precursor solution involves the preparation of batches containing separately the solution of each chemical reagent. Sodium acetate anhydrous (CH_3COONa, 99.995%, Sigma-Aldrich), barium acetate ($(CH_3COO)_2Ba$, ACS reagent, 99%, Sigma-Aldrich) and bismuth (III) acetate ($(CH_3COO)_3Bi$, 99.99+%, Sigma-Aldrich) were

M. Cernea (✉) · A. C. Galca · M. C. Cioangher · C. Dragoi
National Institute of Materials Physics, P.O. Box MG-7, 077125 Bucharest-Magurele, Romania
e-mail: mcernea@infim.ro

G. Ioncea
METAV-R&D S. A., P.O. Box 22, Bucharest, Romania

dissolved in acetic acid (ACS reagent, ≥99.7%, Sigma-Aldrich) under stirring and heating at 85 °C. For the chemical routes which usually combine several cations, a risk of phase separation can occur because the presence of these cations in solution does not preclude the formation of a mixed oxide network. One way to prevent a phase separation is to favor combined condensation rather than self-condensation reactions between the molecular reagents [19]. The main parameters in the solution synthesis are the solubility and the reactivity of alkoxides leading to the formation of a mixed inorganic network in a solvent medium. While sodium alkoxides are non-volatile and poorly soluble solids, bismuth alkoxides are known to exhibit a weak reactivity toward titanium alkoxide [20]. The solutions of sodium acetate, barium acetate, and bismuth acetate in acetic acid were mixed together. Titanium (IV) isopropoxide, 97% solution in 2-propanol ($Ti\{OCH(CH_3)_2\}_4$, Sigma-Aldrich) was mixed with isopropanol in ratio of 1:5. Two equivalents of acetylacetone were added in order to increase the stability of titanium isopropoxide. Then, the titanium (IV)-isopropoxide was added drop by drop under constant stirring to produce a Bi–Na–Ba–Ti complex solution. To this sol, 5% by volume of formamide (*N*,*N*-dimethylformamide, Aldrich) was added in order to minimize the formation of cracks occurring during the drying and the annealing steps [21]. The mixture was finally filtered using a 0.45 μm Nylon membrane (Aldrich). The filtrate was used as the stock solution for the preparation of the films. The substrates used for this study were $Si/SiO_2/TiO_2/Pt$ wafers. Prior to the deposition of the films, the substrates were cleaned by adopting a standard chemical procedure. The films were deposited by spin casting a single coating at 3,000 rpm for 20 s using a spinner. After spin coating, the samples were baked at 200 °C for 2 min to evaporate the solvent, and then at 400 °C for 4 min in air to eliminate organic components. The films were prepared by repeating (10 times) the deposition and pyrolysis cycle. The coated films were finally annealed in air at 700 °C for 1 h in a conventional furnace, for achieving crystallization.

The structure of the film was analyzed by a Bruker D8 Advance X-ray diffractometer. A Woollam Variable Angle Spectroscopic Ellipsometer (VASE) is employed for optical investigation of obtained thin films. The experimental data were acquired in the 0.73–4.5 eV spectral range. Ellipsometry measurements are performed in reflection mode at angles of incidence (AOI) of 45°, 60°, and 75°. The microstructure of the samples was investigated using a FEI Quanta Inspect F scanning electron microscope (SEM). An atomic force microscope (AFM) (MFP 3D SA, Asylum Research) was used to obtain a high resolution image of the surface. DART (Dual AC Resonance Tracking) measurement technique was used for study of the local electromechanical activity at nanoscale size. The small displacement of the BNT thin film induced by the converse piezoelectric effect was measured applying an ac voltage with amplitude of 0.66 V via the PFM tip directly on the film surface without the top electrodes. For electrical measurements, Pt electrodes were deposited on top. Deposition of metallic contacts was made by sputtering, using a metal mask with dimensions of 0.2 mm^2. The ferroelectric hysteresis (*P*-*E*) loop was measured using a

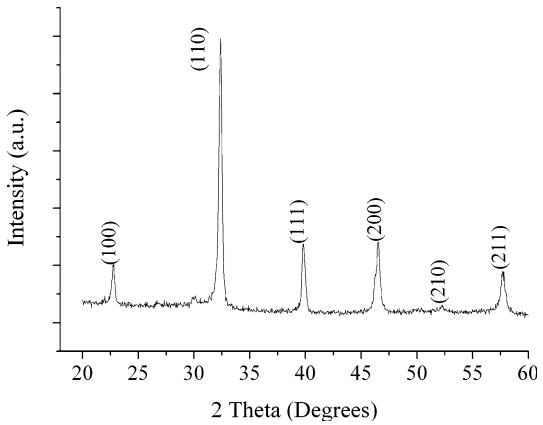

Fig. 1 XRD patterns (CuK_α radiation) of sol–gel processed BNT-$BT_{0.11}$ thin film annealed at 700 °C, 1 h in air

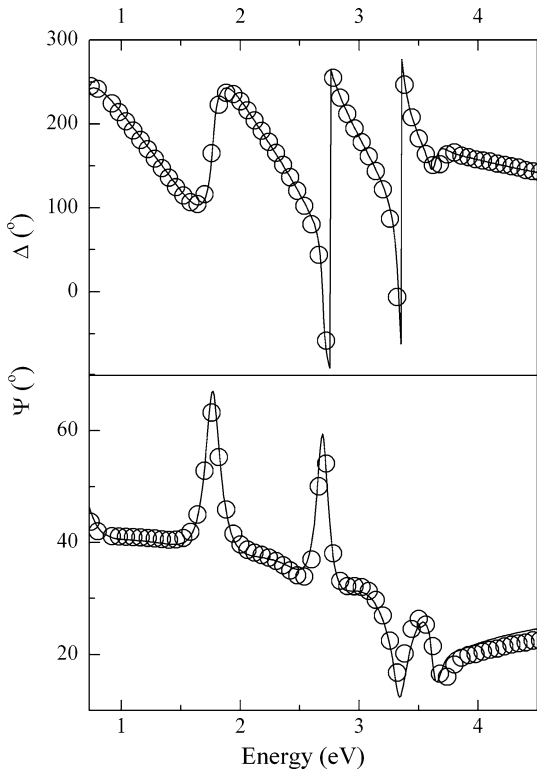

Fig. 2 Experimental and generated spectroscopic ellipsometry data (angle of incidence = 60°) corresponding to the BNT-$BT_{0.11}$ thin film with a thickness of 260 nm

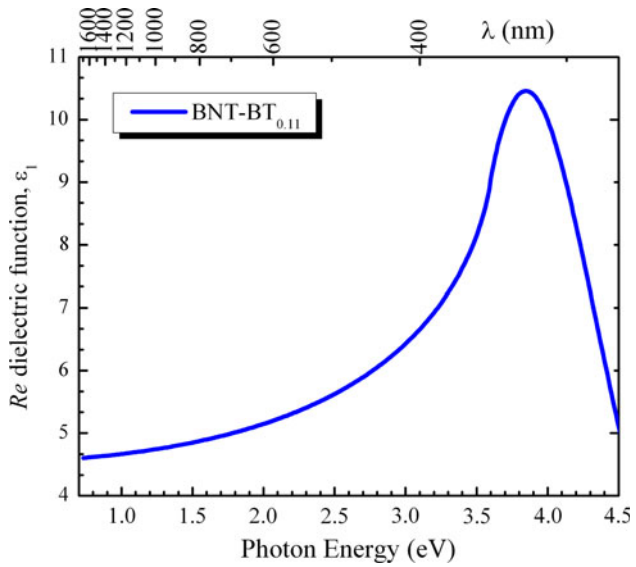

Fig. 3 Real part of dielectric function of BNT-$BT_{0.11}$ thin film

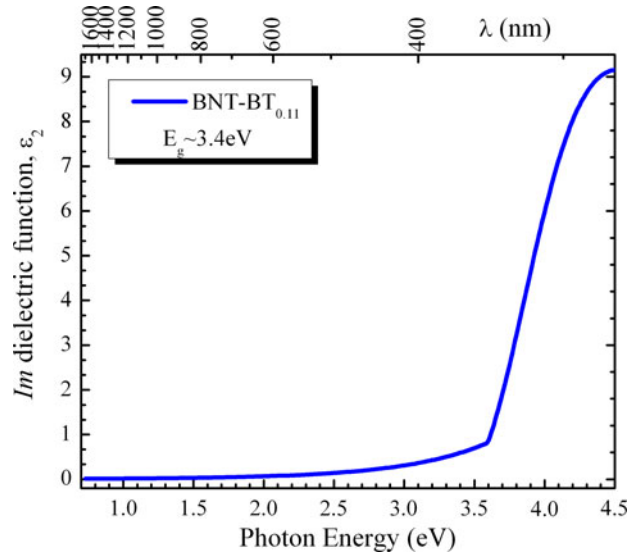

Fig. 4 Imaginary part of dielectric function of BNT-$BT_{0.11}$ thin film

TF Analyzer 2000 equipped with a FE-Module (aixACCT). Dielectric properties of Pt/BNT-$BT_{0.11}$/Pt capacitor were measured at 100 kHz frequency, at room temperature, using a HIOKI LCR-meter. The leakage current through the Pt/BNT-$BT_{0.11}$/Pt capacitors was measured at room temperature using a Keithley 6517A programmable electrometer.

Results and discussion

Structure

The XRD pattern of BNT-$BT_{0.11}$ thin films (Fig. 1) indicates that the films are crystallized on $Bi_{0.5}Na_{0.5}TiO_3$ cubic lattice without preferred orientation.

Spectroscopic ellipsometry

Ellipsometry is used here for the investigation of the dielectric properties (complex refractive index and dielectric function) of BNT-$BT_{0.11}$ thin films. These characteristics are related to a variety of sample properties, including morphology, crystal quality, chemical composition, or electrical conductivity [22]. Ellipsometry is commonly used to characterize film thickness with an excellent accuracy. By using an adequate optical model, thin film thickness and its dielectric function are obtained. The refractive index (or dielectric function) is dependent on the atomic masses and atomic density of each element. This dependence holds in UV–Vis spectral range where the electronic polarization contributes to the value of refractive index [23]. For example, the material studied in this study ($(Bi_{0.5}Na_{0.5}TiO_3)_{0.92}(BaTiO_3)_{0.11}$), has a refractive index weighted by the molar ratio between the two compounds. Assuming the same structural primitive cell parameters, $BaTiO_3$ single crystal has a higher refractive index (2.37906 at 0.7 μm, [24]) than $Bi_{0.5}Na_{0.5}TiO_3$, because half of the relative atomic masses sum of Bi and Na (~115.5)

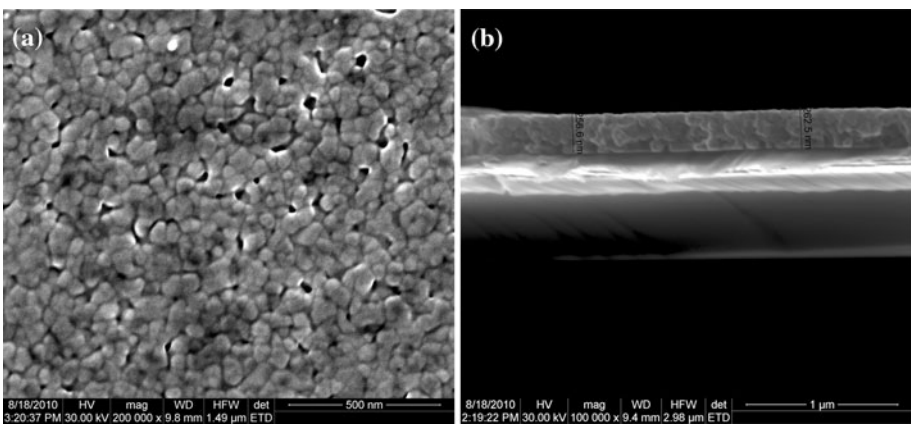

Fig. 5 SEM micrographs of the BNT-$BT_{0.11}$ thin films heated at 700 °C: **a** plain-view image and **b** cross-section image

is smaller than the relative atomic mass of Ba (~137.3). Therefore, a higher concentration of $BaTiO_3$, will give a material with a higher refractive index. To analyze the ellipsometry spectra, a three layer optical model is used, consisting of substrate, thin films, and the top rough layer. The dielectric function of deposited thin film is approximated by using a Cody-Lorentz model [25]. The experimental and fitted data are presented in Fig. 2, whereas the dielectric functions of the obtained thin films are shown in Figs. 3 and 4. Although the Cody-Lorentz model is mainly used to characterize amorphous thin films, in this study is shown that this model is effective also for polycrystalline materials. Due to small crystallite size, there is a high density of grain boundaries 'defects' which are optically active and they produce a Urbach tail of imaginary part of dielectric function (Fig. 4). Moreover, the modeled electronic transition is a macroscopic estimation of all such transitions of grains with different sizes. The refractive index in the transparency range of a polycrystalline material is slightly lower than the refractive index of a single crystal [26]. However, the refractive indices of polycrystalline titanates thin films remain above 2. The band gap E_g of BNT-$BT_{0.11}$ thin films is approximately 3.4 eV.

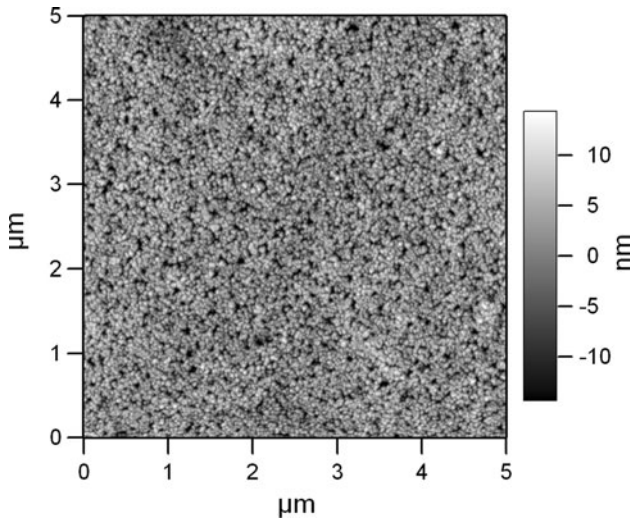

Fig. 6 Atomic force microscopy images of BNT-$BT_{0.11}$ thin film heat-treated at 700 °C

Microstructure

The microstructure of the film surface and cross-section investigated by SEM is shown in Fig. 5a and b.

It can be seen that the film contains a number of clusters which are composed of grains of average size ranging of 50 nm (Fig. 5a). The BNT-$BT_{0.11}$ film is uniform in thickness (Fig. 5b) and its thickness is about 260 nm, in good agreement with that measured by ellipsometry. The films demonstrate a reasonably dense microstructure although there exists a small amount of pores resulting from the burning of the residual organic vehicle in green

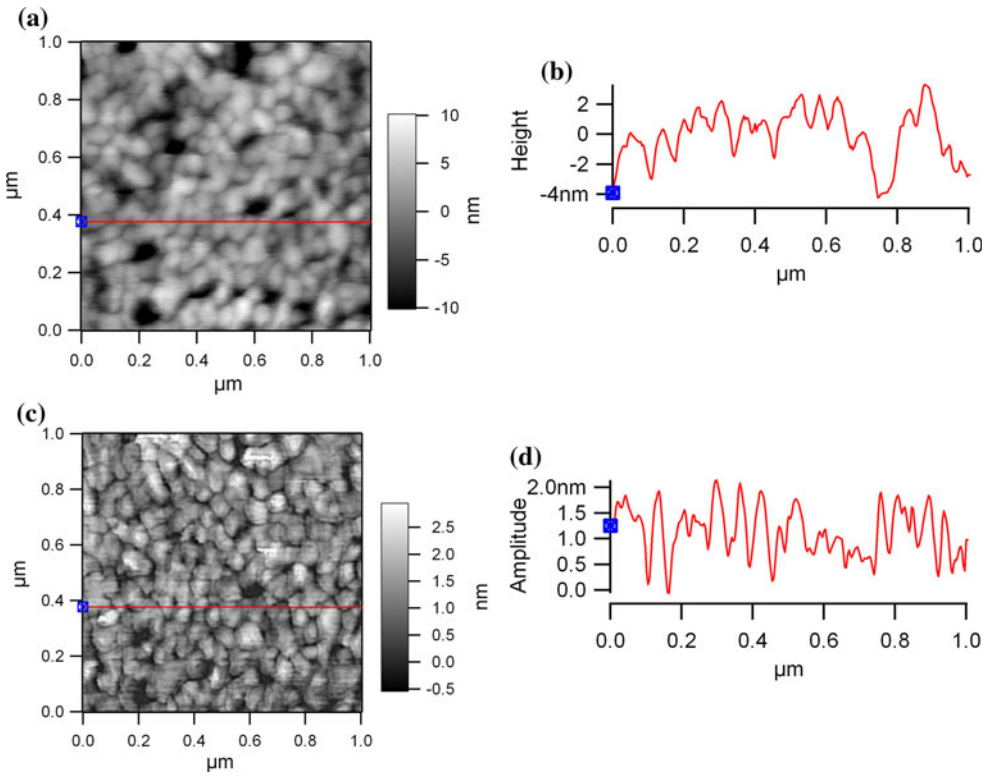

Fig. 7 Morphology image (**a**), piezoresponse image (**b**) and line profile analysis of morphology (**c**), and piezoresponse (**d**) signal of BNT-$BT_{0.11}$ thin film

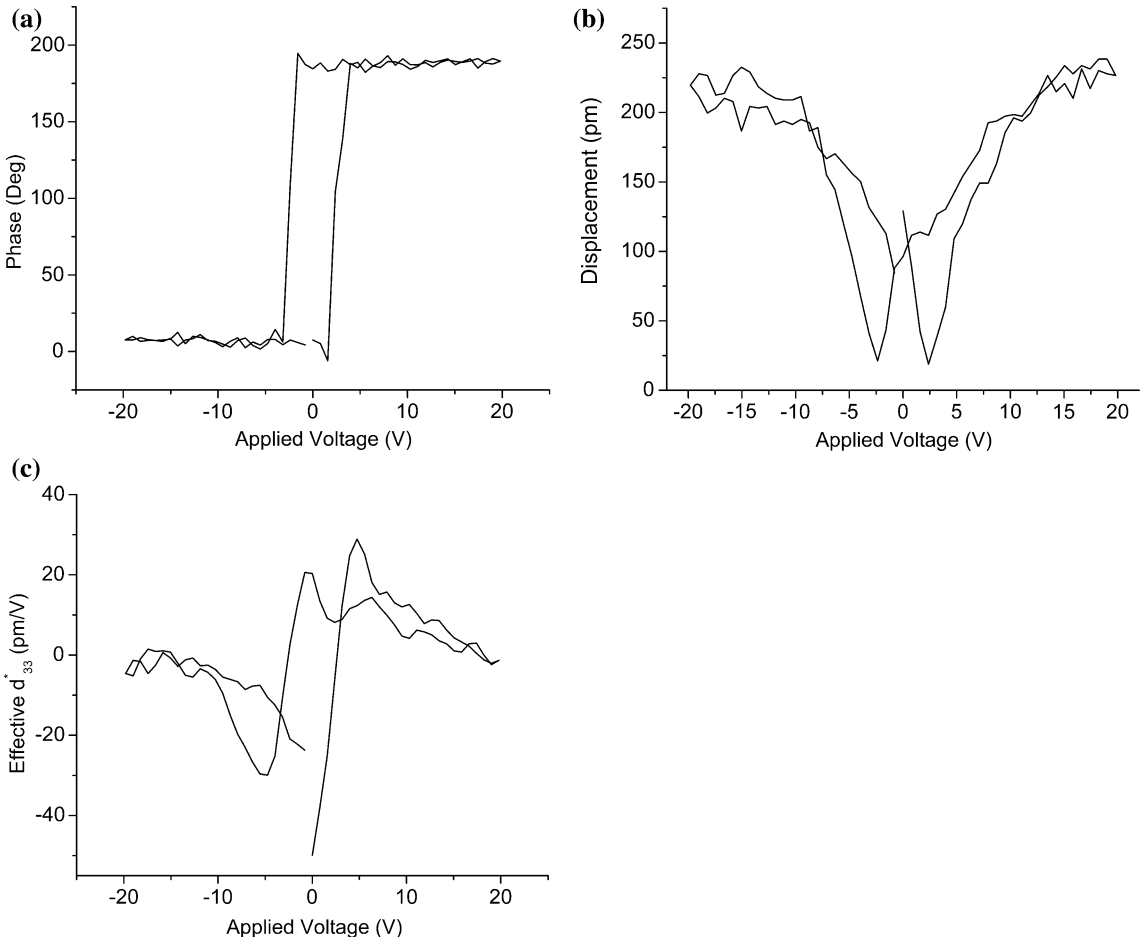

Fig. 8 Switching spectroscopy piezoresponse force microscopy (SSPFM) of BNT-$BT_{0.11}$ thin film: **a** phase-voltage hysteresis loop, **b** amplitude-voltage butterfly loop, and **c** local piezoresponse $d_{33\text{eff}}$ hysteresis loop

films as shown in Fig. 5a. The cross-section and plain-view images of the films revealed that they had a granular structure and the grain size is 40–50 nm.

The surface morphology of the BNT-$BT_{0.11}$ thin films grown on Si–Pt substrate is also observed by AFM (Fig. 6).

A topographic image of the sample shows a very fine grained microstructure with small roughness ($R_{\text{ms}} = 5$ nm) and average grain size of $\sim$40 nm.

One micrometer scan size DART-PFM images (topography and vertical piezoresponse signal) of BNT-$BT_{0.11}$ thin film are shown in Fig. 7a and b, respectively. Line profile analysis of these images is also shown in Fig. 7c and d.

The response amplitude provides a measure of the local electromechanical activity of the surface. Since the vertical PFM technique is sensitive only to the component of polarization normal to the film surface, grains with in-plane polarization (with vanishing out-of-plane polarization) will exhibit an intermediate contrast. Most of the ferroelectric domains have dimensions smaller than grain size as is shown in the line profile of piezoresponse signals (Fig. 7d), indicating that one grain may have a multidomains structure.

The resultant piezoresponse was then measured using a sequence of dc bias up to 20 V superimposed on an ac modulation bias near resonance frequency. Such curves were recorded in different regions (grains). The hysteresis loop between the PFM phase and dc bias, as shown in Fig. 8a, accompanied by a characteristic butterfly loop between PFM amplitude and dc bias, as shown in Fig. 8b indicates the ferroelectric and piezoelectric nature of BNT-$BT_{0.11}$ thin film [27].

As shown in Fig. 8b, the maximum value of effective piezoelectric coefficient $d_{33\text{eff}}$ is approximately 29 pm/V recorded at 5 V applied dc voltage. This value of d_{33} is similar to that of BNT-$BT_{0.02}$ [13].

Figure 9 presents the evolution of the room temperature hysteresis loop of BNT-$BT_{0.11}$ thin film, with an increasing applied voltage, ranging from 10 to 14 V, at a frequency of 10 kHz.

The shape of the hysteresis loops is satisfying but reflecting that the loops are not perfectly saturate.

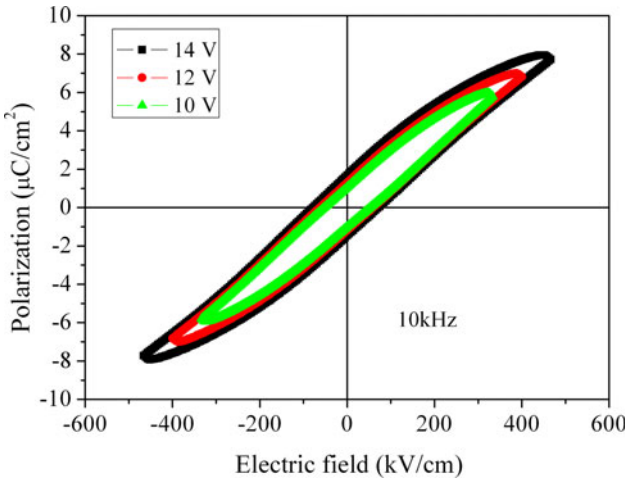

Fig. 9 P-E hysteresis loop of the BNT-$BT_{0.11}$ thin film under various electrical fields

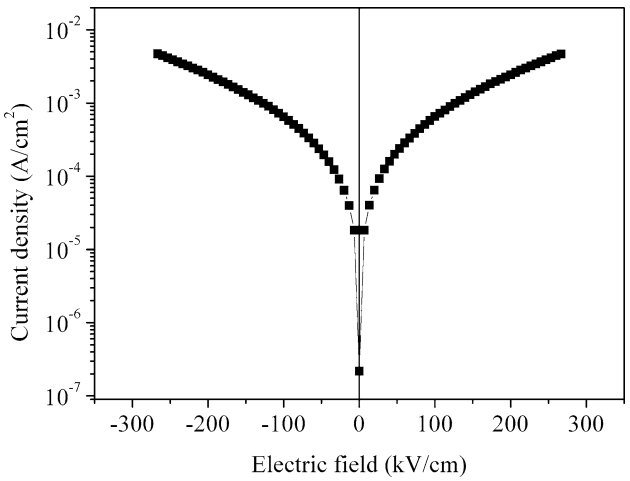

Fig. 10 Current density as a function of electric field for the Pt/BNT-$BT_{0.11}$/Pt thin film capacitor at room temperature

Unsaturation results from the high leakage currents existing in our BNT-$BT_{0.11}$ thin films. The observed remnant polarization P_r and coercive field E_c, are 1.06 μC/cm^2 and 53.39 kV/cm, respectively, at an applied voltage of 10 V and increase to 1.59 μC/cm^2 and 74.85 kV/cm, at an applied voltage of 14 V.

Figure 10 shows the current density J as a function of electric field for the BNT-$BT_{0.11}$ thin film measured at room temperature.

The observed J has a value of about 2.1×10^{-7} A/cm^2 at low electric field (0 kV/cm), and increases significantly to 5.2×10^{-4} A/cm^2 at the electric field of 100 kV/cm. This value is higher to that reported for BNT thin film fabricated by radio-frequency magnetron sputtering, a leakage current density of $\sim 6 \times 10^{-5}$ A/cm^2 measured at an applied electric field of 100 kV/cm [28]. The localized oxygen vacancies trapped at grain boundaries can pin

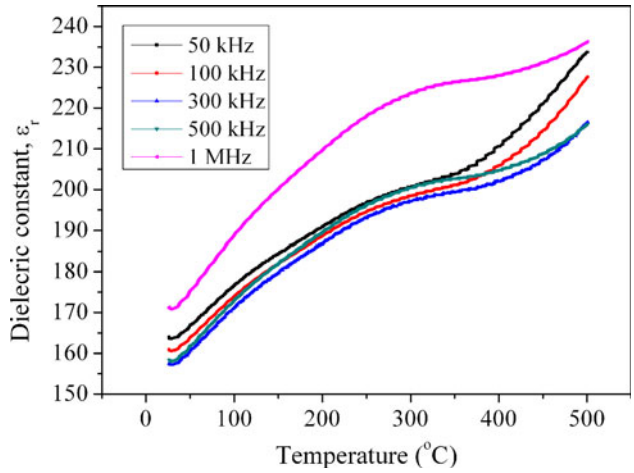

Fig. 11 Temperature and frequency dependence of dielectric constant of the BNT-$BT_{0.11}$ thin film

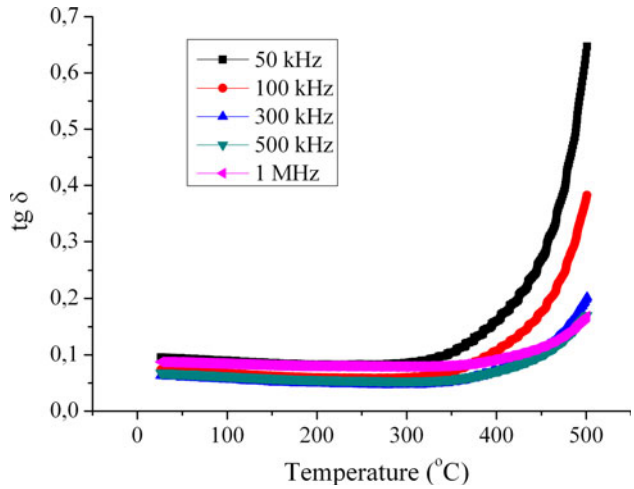

Fig. 12 Temperature and frequency dependence of dielectric loss of the BNT-$BT_{0.11}$ thin film

domains and result in leakage current and polarization degradation, which is a common phenomenon for ferroelectric thin films [28].

The dielectric constant and loss tanδ were measured as a function of frequency and temperature, as shown in Figs. 11 and 12.

The values of dielectric constant and dielectric loss measured at room temperature for BNT-BT_{11} thin film are 164 and 0.095 at 50 kHz. With the increase from 50 to 500 kHz, the dielectric constant and the dielectric loss slightly decrease at first (to 158 and 0.063), and then quickly increases (to 158.5 and 0.067, respectively). This phenomenon is attributed to the presence of the barrier layers between the insulating film and the electrodes. An identical variation with frequency was observed for dielectric constant and dielectric loss at the Curie

temperature. The temperature dependence of dielectric constant presents a broad maximum at $T_c \sim 300$ °C.

Conclusions

$BT_{0.11}$ thin films with the roughness of $\sim$5 nm were prepared by spin coating deposition of the precursor sol. The films are single perovskite phase. By using the spectroscopic ellipsometry, the film thickness was found to be 260 nm, the refractive indices were >2 and the band gap was 3.4 eV for BNT-$BT_{0.11}$ thin films. The results of PFM measurement indicated that the grains have a ferroelectric multidomains structure. The ferroelectric BNT-$BT_{0.11}$ thin films synthesized by sol–gel method suffer from disadvantages related to high leakage current density, which significantly influence the dielectric, ferroelectric, and piezoelectric properties of the films.

Acknowledgement We thank the Romanian National Program PNCDI II, Contract No. 72-153/2008, and the Romanian National Authority for Scientific Research (PN09-450101, Contract No. 45N/1.03.2009) for the financial support.

References

1. Hiruma Y, Watanabe Y, Nagata H, Takenaka T (2007) Key Eng Mater 350:93
2. Zvirgzds JA, Kapostis PP, Zvirgzde JV (1982) Ferroelectrics 40:75
3. Trujillo S, Kreisel J, Jiang Q, Smith JH, Thomas PA, Bouvier P, Weiss F (2005) J Phys 17:6587
4. Chiang YM, Farrey GW, Soukhojak AN (1998) Appl Phys Lett 73:3683
5. Takenaka T, Maruyama K, Sakata K (1991) Jpn J Appl Phys 30:2236
6. Chu BJ, Chen DR, Li GR, Yin QR (2002) J Eur Ceram Soc 22:2115
7. Chen M, Xu Q, Kim BH, Ahn BK, Ko JH, Kang WJ, Nam OJ (2008) J Eur Ceram Soc 28:843
8. Rout D, Moon KS, Rao VS, Kang SJL (2009) J Ceram Soc Jpn 117:797
9. Yilmaz H, Messing GL, Trolier-McKinstry S (2003) J Electroceram 11:207
10. Yilmaz H, Trolier-McKinstry S, Messing GL (2003) J Electroceram 11:217
11. Alonso-Sanjose D, Jimenez R, Bretos I, Calzada ML (2009) J Am Ceram Soc 92:2218
12. Cernea M, Andronescu E, Radu R, Fochi F, Galassi C (2010) J Alloy Compd 490:690
13. Ge W, Liu H, Zhao X, Pan X, He T, Lin D, Xu H, Luo H (2008) J Alloy Compd 456:503
14. Zhang ST, Kounga AB, Aulbach E, Deng Y (2008) J Am Ceram Soc 91:3950
15. Cheng HW, Zhang XJ, Zhang ST, Feng Y, Chen YF, Liu ZG, Liu GX (2004) Appl Phys Lett 85:2319
16. Dinescu M, Craciun F, Scarisoreanu N, Verardi P, Moldovan A, Purice A, Sanson A, Galassi C (2005) J Phys IV France 128:77
17. Scarisoreanu N, Craciun F, Ion V, Birjega S, Dinescu M (2007) Appl Surf Sci 254:1992
18. Zhang DZ, Zheng XJ, Feng X, Zhang T, Sun J, Dai SH, Gong LJ, Gong YQ, He L, Zhu Z, Huang J, Xu X (2010) J Alloy Compd 504:129
19. Brinker J, Scherer GW (1990) Sol-gel science: the physics and chemistry of sol-gel processing. Academic Press Inc, Boston
20. Ryu SO (1999) Synthesis and characterization of ferroelectric $(1-x)SrBi_2Ta_2O_9-xBi_3TaTiO_9$ thin films for non-volatile memory applications. http://scholar.lib.vt.edu/theses/available/etd-050699-154541/unrestricted/Chapter5.pdf
21. Chang DA, Choh YH, Hsieh WF, Lin P, Tseng TY (1993) J Mater Sci 28:6691. doi:10.1007/BF00356416
22. Fujiwara H (2007) Spectroscopic ellipsometry: principles and applications. Wiley, West Sussex
23. Bass M (ed) (2009) Handbook of optics, 3rd edn, vol 4: optical properties of materials, nonlinear optics, quantum optics. McGraw-Hill Comp, Inc., New York
24. Ferlauto AS, Ferreira GM, Pearce JM, Wronski CR, Collins RW, Deng X, Ganguly G (2002) J Appl Phys 92:2424
25. Stan GE, Pasuk I, Galca AC, Dinescu A (2010) Dig J Nanomater Biostruct 5:1041
26. Ma C, Tan X (2010) Solid State Commun 150:497
27. Zhou ZH, Xue JM, Li WZ, Wang J, Zhu H, Miao JM (2004) Appl Phys Lett 85:804
28. Takenaka T, Sakata K (1989) Ferroelectrics 95:153